RSC Advances

PAPER

View Article Online
View Journal | View Issue

Cite this: *RSC Adv.*, 2016, **6**, 84837

Preliminary study of a novel nanofiber-based valve integrated tubular graft as an alternative for a pulmonary valved artery

Jialing Zhang,†[a] Jun Du,†[b] Dekai Xia,[a] Jinlong Liu,[ac] Tong Wu,[d] Jing Shi,[b] Wei Song,[d] Dawei Jin,[a] Xiumei Mo*[d] and Meng Yin*[a]

A suitable valve scaffold is necessary to replace the pulmonary artery in congenital heart disease (CHD) treatment, especially for children. For clinical and long-term success, biomechanics, biocompatibility, functionality and growth potential should be together taken into consideration to construct a tissue-engineered valve scaffold. In this study, a thermally induced phase separation (TIPS)-based strategy combining a three-dimensional (3D) printing mold was utilized to rapidly fabricate poly(L-lactic acid)/poly(L-lactide-*co*-ε-caprolactone) (PLLA/PLCL) valve integrated scaffolds with a bionic structure. The novel valve integrated scaffolds exhibited favorable mechanical properties, in comparison to the porcine physiological pulmonary artery. Moreover, it satisfied functional performance in fluid, as demonstrated by the computational fluid dynamics simulation results. H&E and Masson staining further confirmed its excellent biocompatibility and vascularization *in vivo*, and fiber morphology and collagen production indicated its abundant extracellular matrix (ECM) secretion as well. Hence, the overall results supported that this original strategy was an efficient method to fabricate valve integrated scaffolds with potential value for clinical application of complex CHD.

Received 23rd June 2016
Accepted 1st September 2016

DOI: 10.1039/c6ra16292d

www.rsc.org/advances

Introduction

A variety of complex congenital heart diseases (CHD) with severe right ventricular outflow tract (RVOT) obstruction or RVOT interruption are a serious and increasing clinical burden that affects patients at all stages and walks of life, which requires surgical reconstruction of the pulmonary artery.[1] Under normal physiological conditions, the pulmonary valved artery maintains a unidirectional blood flow by opening and closing valves. The valves allow blood to flow into the lungs during systole and prevent back flow into the right ventricular in diastole. An abnormal flow pattern has been suspected of resulting in heart failure in the long term.[2] In order to prevent the reflux of blood flow in the pulmonary artery, a valve conduit replacement is considered to be the most prevalent treatment approach for these diseases.

A major criterion for a valve conduit substitution is that the valves and conduit must mimic the physiological function of the native pulmonary valve. The pulmonary valves consist of three leaflets with significantly special geometries. Several studies highlighted that the geometry of the valve leaflets was critical to efficient hemodynamics[3,4] and durability.[5] In addition to geometry, spatial and mechanical property is also critical for function. However, the site which bonded valve leaflets with the wall of conduit is significantly more rigid,[6–8] so it is important to develop a substitution that valve leaflets and the wall is integrated. Conduit types include bioprostheses in Dacron tubes, xenografts, and pulmonary homografts.[9] Although pulmonary homograft was usually the most effective alternative, it was usually difficult to be favored due to the shortage of donors and its propensity for obstruction and calcification.[10] Simultaneously, the xenograft replacement has been often limited by the immunological reaction after implantation. Even worse, during the replacement therapy among children, the main shortcoming of the biological valve conduit is the lack of growth capability, repair and the remodeling of the substitute valve. Therefore, the clinical utility of these valve conduit substitutions is limited, particularly in growing children. There still remains a clear clinical need for a functional valve scaffold.

Tissue engineering (TE)-based approaches have shown tremendous potential to overcome these limitations by the development of biodegradable scaffolds, which provide biomechanical and biochemical properties competitive with the

[a]*Department of Cardiothoracic Surgery, Shanghai Children's Medical Center, Shanghai Jiao Tong University School of Medicine, Shanghai 200127, China. E-mail: mengyinmdphd@163.com*

[b]*Imaging Diagnosis Center, Shanghai Children's Medical Center, Shanghai Jiaotong University School of Medicine, Shanghai 200127, China*

[c]*Institute of Pediatric Translational Medicine, Shanghai Children's Medical Center, Shanghai Jiao Tong University School of Medicine, Dongfang Road, Shanghai, China*

[d]*College of Chemistry, Chemical Engineering and Biotechnology, State Key Laboratory for Modification of Chemical Fibers and Polymer Materials, Donghua University, Shanghai 201620, China. E-mail: xmm@dhu.edu.cn*

† Jialing Zhang and Jun Du contributed equally to this work.

native tissue. Tissue engineered scaffolds aim at mimicking the natural extracellular matrix (ECM) both structurally and functionally to provide a suitable biophysiological microenvironment for tissue regeneration.[11] Thermally induced phase separation (TIPS) was a simple and versatile method which widely used for the fabrication of porous scaffolds for tissue engineering and related applications.[12–14] TIPS-based vascular scaffolds have specific advantages because they can achieve synergetic mechanics and biology function in accordance with the requirements in the hemodynamic environment.[15] Additionally, TIPS-based methodology can be trusted to obtain the polymer scaffold with a controlled shape and size.

For potential clinical use, a valve scaffold for tissue engineering should be biocompatible, nonthrombogenic, nonimmunogenic, and possess appropriate biomechanical properties as well.[16–18] The comprehensive property of a valve scaffold depends essentially on the inherent quality of the selected polymer.[19] As one of the few polymers that can be fabricated into nanofibrous scaffold *via* TIPS technique, poly(L-lactic acid) (PLLA) has been widely used due to its good biocompatibility and biodegradability.[20,21] Likewise, poly(L-lactide-*co*-ε-caprolactone) (PLCL) copolymers have attracted widespread attentions for use in vascular tissue engineering owing to its inherent elasticity and flexibility.[22–24] The nanofibrous scaffolds using PLLA/PLCL mixtures with appropriate compositions by TIPS showed desirable structural and mechanical properties for viable vascular application.[15]

In this study, a TIPS-based method combining 3D printer was developed to fabricate the tri-leaflet valve integrated tubular scaffold for surgical replacement of pulmonary artery. An electronic data were acquired by computer aided design (CAD) system to obtain a 3D-shape and size mold with accurate geometry produced by the 3D printer within several processing hours. Then a TIPS-based strategy was carried out to fabricate a valve integrated scaffold combining with the 3D mold. The structural and mechanical properties of the resultant scaffolds were evaluated, and the potential application of such valve scaffolds was also evaluated by computational fluid dynamics simulation with respect to their valuvalar performance. The biocompatibility of graft *in vivo* was evaluated by subcutaneous implantation in mice.

Materials and methods

Materials

PLLA (1.93 dL g^{-1} inherent viscosity) and PLCL (50 : 50, 1.5 dL g^{-1} inherent viscosity) were purchased from Daigang Biomaterials Inc (Jinan, China). PLLA was purified by dissolving in chloroform and recrystallized in ethanol and then dried for use. Tetrahydrofuran (THF) were purchased from Sigma-Aldrich (Shanghai) Trading Co., Ltd. (Shanghai, China). All other chemicals were of analytical grade and obtained from Sinopharm Chemical Reagent Co., Ltd. (Shanghai, China).

Mold preparation by 3D printing technology

The mold was designed based on the geometry of a CAD design diagram (Fig. 1A) and prepared using a 3D digital printer (Objet 260 Connex), which consisted of three parts: the convex and pulmonary arterial trunk side mandrel portion (diameter 14 mm; length 40 mm), the mandrel part of concave and heart

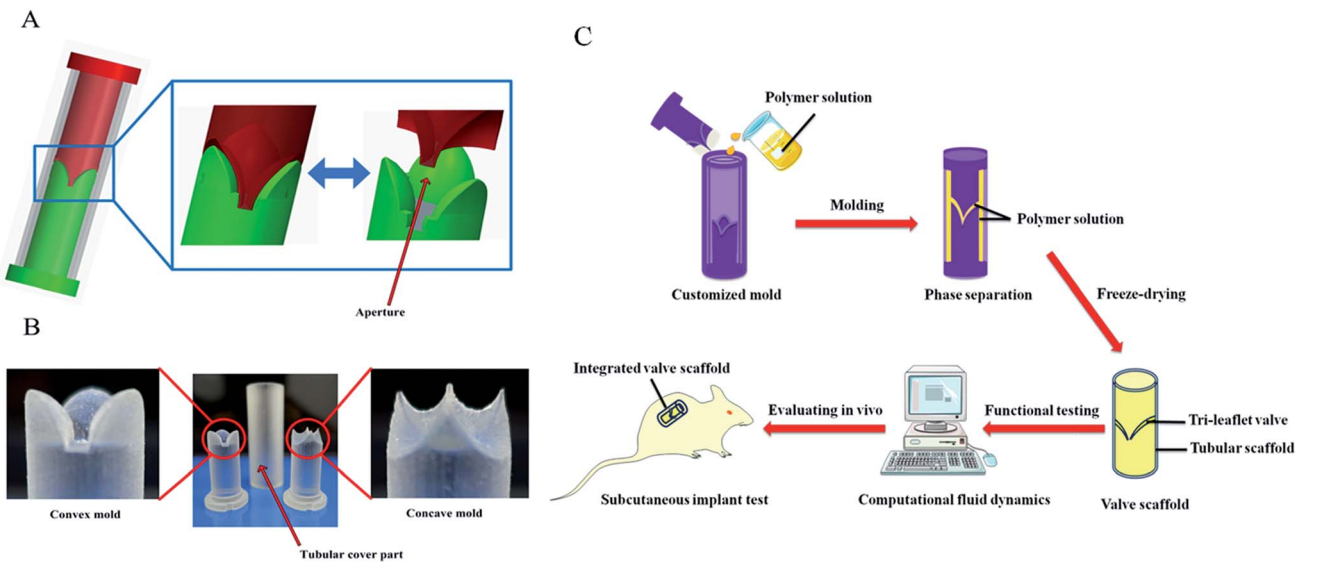

Fig. 1 (A) Design diagram of the assembled mold by CAD. A convex-shaped section (diameter 14 mm; length 40 mm) was connected with a concave-shaped section (diameter 14 mm; length 40 mm) with a small aperture (red arrow) of 0.1 mm. Corolla-like leaflets were processed at the connecting part. The bonding part was inserted into a tubular cover scaffold part (internal diameter 16 mm; thickness 1 mm; length 80 mm). (B) Photo of the assembled mold produced by a 3D digital printer. (C) Schematic illustration of the experimental procedures for fabricating the tri-leaflet valve integrated tubular scaffold. The prepared PLLA/PLCL/THF mixture polymer solution was first poured into a pre-heated customized cylindrical chamber mold and phase separated at −80 °C for 12 h. Then the polymer scaffold was solvent exchanged with ice/water mixture, a tri-leaflet valve integrated tubular scaffold was obtained through freeze-drying. After testing its valuvalar performance *via* computational fluid dynamics, the resultant valve scaffold was implanted subcutaneous into nude mice.

chamber side (diameter 14 mm; length 40 mm), and the outer part of the cylinder section (internal diameter 16 mm; thickness 1 mm; length 80.1 mm) (Fig. 1B). The convex-shaped section connected concave-shaped section with a small aperture about 0.1 mm between the two parts. The final mold was obtained by inserting the combined central rod parts into a tubular cover scaffold part, and was manufactured for the formation of tri-leaflet valve integrated tubular scaffold with the leaflets in the open position (Fig. 1B).

Fabrication of tri-leaflet valve integrated scaffolds

The valve integrated scaffolds were fabricated by TIPS for material characterization and *in vitro* studies. For valve scaffolds preparation, the special mold described above was used, which theoretically produced valve integrated scaffolds with dimensions of 14 mm inner diameters, 1 mm in wall thickness and about 0.1 mm in valve thickness. As schematic illustration of the experimental procedures shown in Fig. 1C, PLLA and PLCL with satisfied weight ratios (40 : 60) were dissolved in THF at 60 °C until homogeneous solutions (10% w/v) were obtained, and then immediately poured into pre-heated customized mold (60 °C). The obtained polymer blend solution was phase separated at −80 °C for 12 h and then immersed into an ice/water mixture to exchange THF for 48 h, changing the ice/water mixture three times per 24 h. The polymer gel was removed from water and subsequently freeze-dried for 48 hours. Thus obtained the valve integrated scaffolds. Computational fluid dynamics (CFD) was employed to evaluate its performance, and subcutaneous implant test was performed in mice ultimately (Fig. 1C).

Valve scaffolds characterization

The PLLA/PLCL scaffolds were fractured after being frozen in liquid nitrogen for several minutes. The specimens were sputter coated with gold using a sputter coater and then observed under a scanning electron microscope (SEM) (JEOL JSM-5600, Japan) at 10 kV. Image analysis software (Image-J, National Institutes of Health, USA) was applied to analyze the average fiber diameter ($n = 100$) and the average pore diameter ($n = 100$) under lower magnification.

Mechanical properties

All samples were prepared for the same size (30 mm × 10 mm, $n = 6$), and tensile mechanical properties were characterized by a universal materials testing machine (3345, Instron, MA, USA) at ambient temperature of 22 °C and a relative humidity of 50%. A crosshead speed of 10 mm min^{-1} was used for all the samples tested until breakage, and a stress–strain curve was then generated. The Young's modulus of each sample was calculated based on the slope of the stress–strain curve. The walls of aortic and pulmonary artery from porcine were used as controls.

Compression testing was performed on the tubular scaffolds (10 mm of length, $n = 3$) using the artificial biological pipeline compressed elasticity tester (LLY-06D, YuanMore, China), and the compression speed was 0.2 mm s^{-1}. For continuous compression test, each data should be repeated 10 times.

CFD & CSD analysis

The valve design should be satisfied with the mechanical requirement for the valve movement. Therefore, the techniques of computational fluid dynamics (CFD) and computational structural dynamics (CSD) were employed for the investigation of hemodynamics, valve deformation and stress analysis. We evaluated these properties under the average cardiac output of child in one cardiac cycle (2 L min^{-1}).

We assumed blood to be a Newtonian fluid with constant density ($\rho = 1060$ kg m^{-3}) and viscosity ($\mu = 4.0 \times 10^{-3}$ Pa s). The 3D incompressible Navier–Stokes equations were solved, which are described as below,

$$\begin{cases} \rho \dfrac{\partial U}{\partial t} + \rho(U \cdot \nabla)U - \mu \nabla^2 U + \nabla p = 0 \\ \nabla \cdot U = 0 \end{cases} \quad (1)$$

where p is the pressure, $U = U(u_1, u_2, u_3)$ is the velocity vector, ρ and μ are blood density and viscosity, and t is time. The standard k–ε model was employed to solve the complex turbulence flows around valves.

We generated a computational mesh for numerical solution of the equations describing the blood flow. The grid-generation software, ANSYS®-ICEM 14.5, was applied to discretize the computational domain with tetrahedral grids. To find the best mesh for CFD analysis, we performed grid-independent verification. In the present study, we used total elements 2 623 893, and the total nodes 628 176 for calculations. The finite volume solver package ANSYS®-CFX 14.5 was applied to solve the physiologic flow in the model. The CSD investigation was done for the analysis of valve deformation and stress. The properties of valve material were obtained by experiments. Young's modulus and Poisson's ratio were set to 4.5 MPa and 0.45. The simulation was performed by ANSYS®-ANSYS14.5. When the relative variation of the calculated quantities between two successive iterations was smaller than the pre-assigned maximum residence 10^{-4}, the calculation was considered convergence for both CFD and CSD.

In vitro biodegradability

The PLLA/PLCL scaffolds were cut into tubes with 20 mm length for biodegradability tests within a scheduled time (35 days). The samples were placed in lipase solution (100 U mL^{-1}) using a 37 °C temperature oscillation shaker. SEM was used to observe morphological changes during the degradation process. The mass remaining percentages were calculated using the following equation by the gravimetrical method:

$$\text{Mass remaining (\%)} = W_1/W_0 \times 100\%$$

where W_0 is the initial weight and W_1 is the dry weight after biodegradation.

Subcutaneous implantation

All experimental protocols were approved by the Animal Care and Experiment Committee of Shanghai Jiao Tong University School of Medicine. Twenty male nude mice (7 weeks old) were

purchased from Shanghai Slaccas Experimental Animal Ltd. (Shanghai, People's Republic of China), which were selected for subcutaneous implantation in this experiment, and PLLA/PLCL scaffolds were prepared for subcutaneous implantation in 10 weeks. Before implantation, the targeted scaffolds were sterilized with ethylene oxide. The mice were anesthetized by intraperitoneal injection of chloral hydrate (400 mg kg^{-1}), and the implantation sites on the back of mice were disinfected using iodine solution. Two subcutaneous pockets were created using a surgical scissor on each side of dorsa. One sample (14 mm in inner-diameter, 20 mm in length) was implanted into each pocket. Then the incisions were sutured.

Histological staining

After gross examination, the samples harvested from all the groups were subjected to histological examinations. The samples were fixed in 4% paraformaldehyde, embedded in paraffin, and then sectioned into 5 μm sections. The sections were stained with hematoxylin and eosin (H&E), and Masson's trichrome to assess tissue structure.

Statistics analysis

Statistics analysis was performed using origin 8.0 (Origin Lab Inc., USA). All the values were averaged at least in triplicate and expressed as means ± standard deviation (SD). Statistical differences were determined by the analysis of one-way ANOVA and differences were considered statistically significant at $p < 0.05$.

Results

Preparation of mold

Before fabricating the nanofibrous valve integrated scaffolds, a specially designed mold was necessarily manufactured. Fig. 1A and B shows the fabrication procedure of the specially designed mold parts. Firstly, a diagram (Fig. 1A) was designed elaborately by computer aided design (CAD) for the following 3D printing process to obtain a customized mold. The shape of the convex or concave parts in this model was designed to mimic the normal form of the physiological tri-leaflet in pulmonary valves, which were wrapped by an isometric hollow conduit. Then the mold assembled by three parts was precisely produced by 3D printer within several hours (Fig. 1B). The mold, comprised of a convex-shaped rod, a concave-shaped rod, and a tubular cover scaffold part, was made by a type of special plastic, which could tolerate extreme temperatures and had chemically inert with both PLLA/PLCL and tetrahydrofuran. These characteristics played critical roles in the process of following TIPS-based experimental production. There was an annulus space between the rods and tubular conduit for the formation of the valve scaffold wall. Two rod-like parts were placed on a same section with a small aperture for tri-leaflets formation.

Morphology and structure of tri-leaflet valve integrated tubular scaffold

Fig. 1C represents the scheme of experimental procedure for fabricating the PLLA/PLCL valve integrated scaffolds *via* TIPS technique. Ultimately, a tri-leaflet valve integrated scaffold was manufactured with multitudinous micropores. As shown in Fig. 2A, the achieved valve scaffold was biomimetic completely, whose valves and wall were well-formed. Inside the scaffold, three separate leaflets were appeared to be almost identical in structure and quality, which were connected at the commissure. The dimension of obtained valve integrated scaffold had been measured, which revealed that the average inner diameter was 14 ± 1 mm and wall thickness was 0.9 ± 0.1 mm. Meanwhile, it had a 0.1 mm average thickness for valves. In general, the resultant valve integrated scaffold had a morphological architecture similar to the physiological valve vascular in order to acquire excellent performance.

Fig. 2B shows the SEM micrograph of the prepared PLLA/PLCL valve scaffold with a certain ratio of 40 : 60. The scaffold exhibited nanofibrous network structure with interconnected micropores. Some study showed that cell infiltration and the formation of capillary-like structures were evidently promoted on nanoyarn scaffolds with a larger pore size.[25] In this way, our scaffold provides a possibility for tissue regeneration of pulmonary artery. Fig. 2C is the fiber diameter distribution of PLLA/PLCL valve scaffolds. The average fiber diameter was 0.64 ± 0.35 μm, demonstrating that it closely resembled the nanoscale dimension of native ECM. Fig. 2D illustrates the pore size distribution between fibers in PLLA/PLCL valve scaffolds. According to our observation, the pore size underwent a wider distribution, ranging from 500 nm to 3000 nm. The averaged pore diameter was about 1.50 ± 0.67 μm.

Mechanical properties

The mechanical properties of the PLLA/PLCL valve integrated scaffolds were characterized by tensile testing. Fig. 3A shows the typical tensile stress–strain curves of PLLA/PLCL scaffolds, the walls of aortic and pulmonary artery from porcine were served

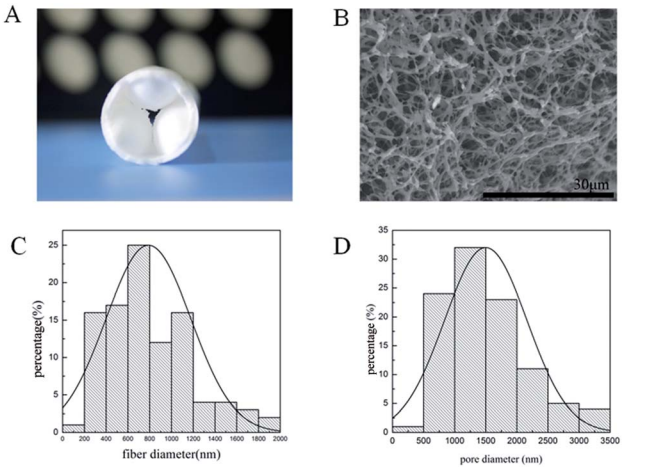

Fig. 2 Morphological architecture of the resultant tri-leaflet valve integrated tubular scaffold (A) and the SEM images of the cross-section of PLLA/PLCL valve nanofibrous scaffolds (B), the corresponding fiber diameter distributions (C) and pore diameter distributions (D) of PLLA/PLCL scaffolds.

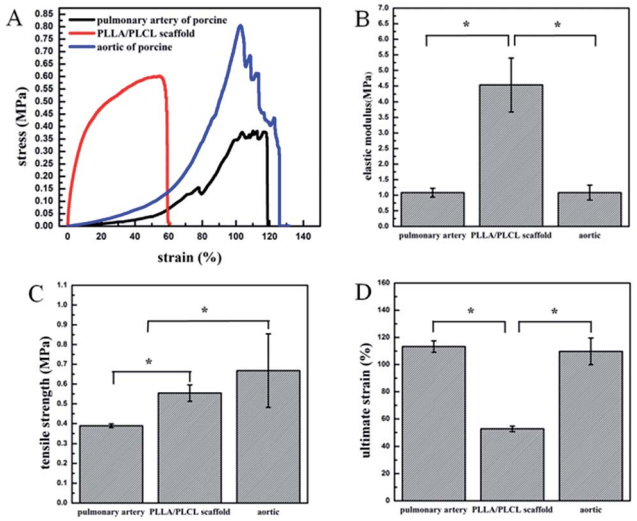

Fig. 3 Typical stress–strain curves of PLLA/PLCL scaffold and the walls of aortic and pulmonary artery from porcine (A). Histogram of elastic modulus (B) and tensile strength (C) and ultimate strain (D) of PLLA/PLCL scaffolds and the aortic and pulmonary artery from porcine.

as controls. The tensile properties including elastic modulus, tensile strength and ultimate strain were illustrated in Fig. 3B–D, which were obtained from the stress–strain curves respectively. As shown in Fig. 3B, the conduit part of PLLA/PLCL valve scaffolds, pulmonary artery, and aortic have elastic moduli of 4.53 ± 0.86, 1.08 ± 0.14, 1.08 ± 0.24 MPa, respectively. In terms of tensile strength, PLLA/PLCL scaffold (0.56 ± 0.04 MPa) was between the pulmonary artery (0.38 ± 0.01 MPa) and aortic (0.67 ± 0.19 MPa) (Fig. 3C). This indicated that our resulting PLLA/PLCL scaffolds were significantly more robust than a physiological pulmonary artery, which could provide sufficient mechanical support for blood pressure in the use of pulmonary valved artery replacement. However, the ultimate strain of PLLA/PLCL scaffold was lower than that of aortic wall and pulmonary artery (Fig. 3D).

In addition, the compression performance of the prepared PLLA/PLCL scaffolds was observed. Fig. 4A shows the radial compressive stress–strain curve for our scaffolds along the loading direction. PLLA/PLCL scaffolds received the maximum pressure of 0.51 N along with maximum compression distance, and its elastic recovery rate was 75.53%. Fig. 4B is the multicycle radial compressive stress–strain curves of 10 cycles on PLLA/PLCL scaffolds. The maximum pressure was 0.59 N with an elastic recovery rate of 79.40% at the first cycle. When repeated to the 10th, the maximum pressure was 0.50 N, and the elastic recovery rate was 73.20%. Therefore, the PLLA/PLCL scaffolds showed a desirable toughness when loaded with pressure.

Hemodynamics analysis

Valvular functioning of scaffolds was evaluated *via* the techniques of computational fluid dynamics (CFD) at a flow rate closed to the average blood velocity of physiological pulmonary artery in children. Fig. 5A shows the CAD geometry of our designed valves. Fig. 5B displays the computational mesh for numerical solution of the equations describing the blood flow. Fig. 5C shows the streamline distribution at the instant of valve opening. Obvious flow statuses were observed between the two sides of the valve. At this state, there was a rapid flow smoothly passing through the whole conduit along the flow direction. Crucially, most of the reverse flow was effectively blocked because of the tri-leaflet valve, and a vortex developed at the bottom of valve.

The structure of every single leaflet was investigated using the technique of computational structural dynamics (CSD). In Fig. 5D, when valve was used to resist the back-flow, the maximum deformation occurred around one quarter and three-

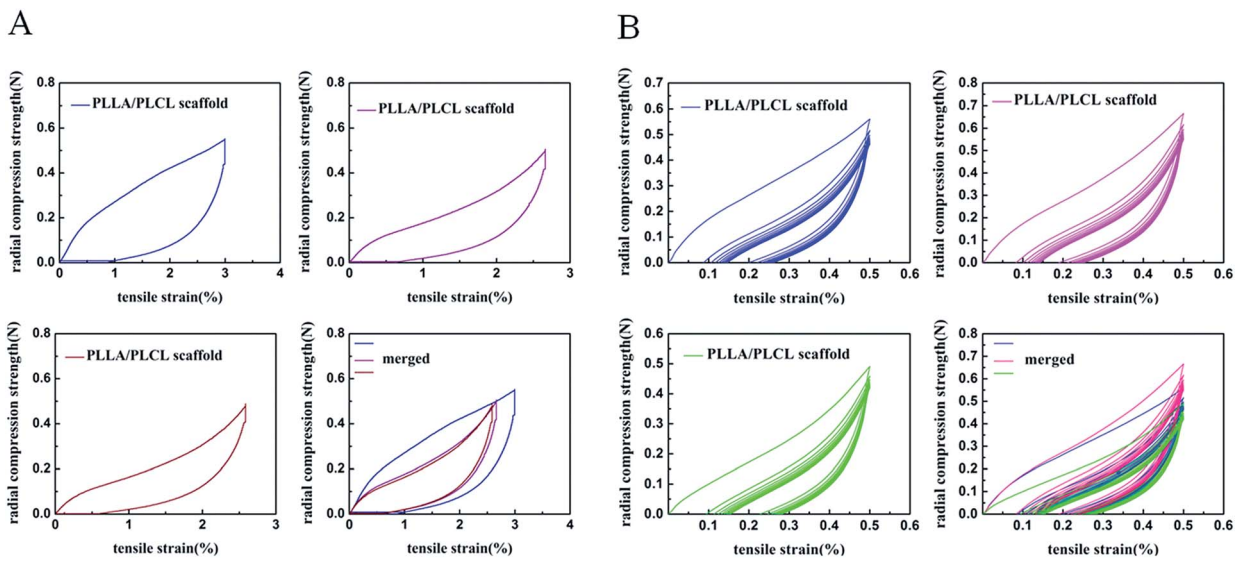

Fig. 4 Radial compression test results of PLLA/PLCL scaffolds under compressing and releasing cycles. (A) Radial compressive stress–strain curves of one cycle along the loading direction; (B) multicycle stress–strain curves of PLLA/PLCL scaffolds during repeated compressions.

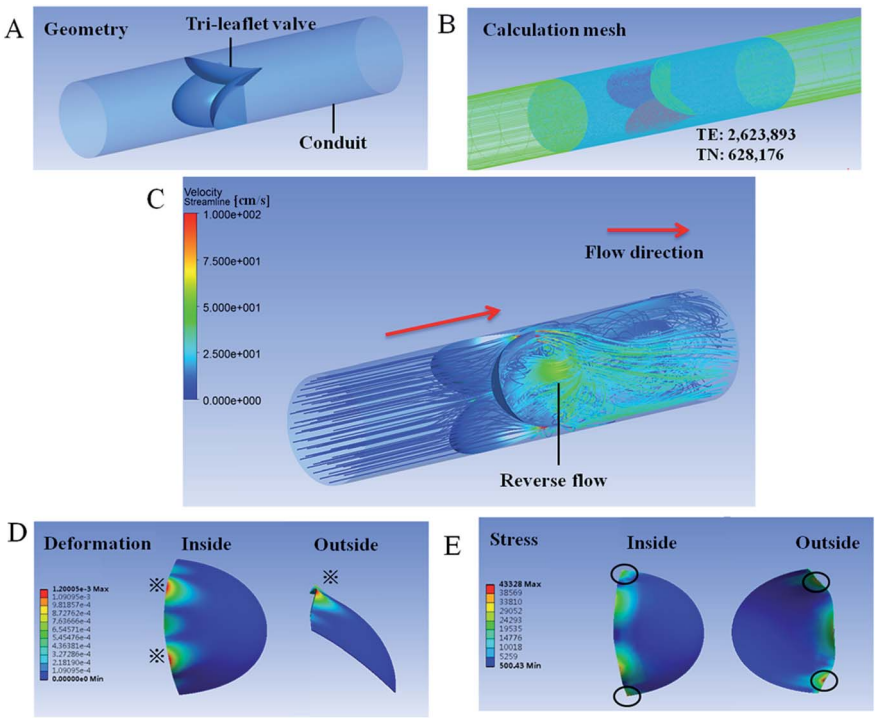

Fig. 5 Design evaluation by CFD and CSD. (A) Valve geometry designed by CAD; (B) mesh generation for numerical analysis; (C) streamline distribution; (D) structural deformation; (E) stress distribution. TE means total element; TN means total node. Asterisks indicate the maximum deformation positions. Circles indicate the higher-stress areas.

quarter area of free edge inside, and midrange of free edge outside, respectively. Accordingly, this tendency also emerged in stress-analysis scope, as shown in Fig. 5E. It indicated a rather remarkable fact that the corners of leaflet also endured relative higher stress when worked adequately.

In vitro biodegradability

SEM micrographs of PLLA/PLCL scaffolds after degradation in lipase solution for 7, 21 and 35 days are shown in Fig. 6A–C, respectively. The structural integrity of the PLLA/PLCL porous scaffold changed during degradation process, which accompanied with the outward diffusion of degradation products, and mass loss of the scaffold (Fig. 6D).

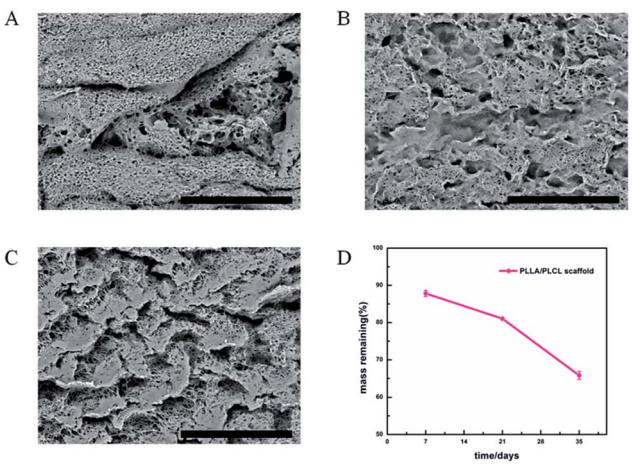

Fig. 6 SEM images of PLLA/PLCL scaffolds after biodegradation for 7 days (A), 21 days (B) and 35 days (C); bar = 50 μm. (D) The corresponding mass remaining of PLLA/PLCL scaffolds.

Histological analysis after subcutaneous implantation

PLLA/PLCL valve scaffolds were implanted subcutaneously into nude mice for 10 weeks. Histological analysis of transverse sections at the middle sites was performed by H&E staining and Masson's trichrome staining (Fig. 7 and 8). As shown, host cells migrated and infiltrated into the scaffolds after subcutaneous implantation. A thin cell layer and fibrous encapsulation was formed surrounding the graft wall (Fig. 7). Meanwhile, collagen fibers were produced on the surface of scaffolds by the infiltrated cells, which were evaluated visually by the Masson's trichrome staining in Fig. 7. As expected, the collagen production increased gradually with time, and abundant collagen was observed in the scaffolds at 10 weeks (Fig. 7C and D), which could provide appropriate microenvironments for tissue regeneration. In addition, lots of new capillaries were found especially on the lumen surface of PLLA/PLCL scaffolds (Fig. 8).

Discussion

A suitable valve scaffold is necessary in a wide range of complex cardiovascular malformations, especially in infancy and early childhood. Widespread efforts have been made with decellularized allogeneic valves, but they showed failure due to severe shortage of donors and pathological calcification, particularly in very young patients.[26,27] Much worse, such valve scaffolds

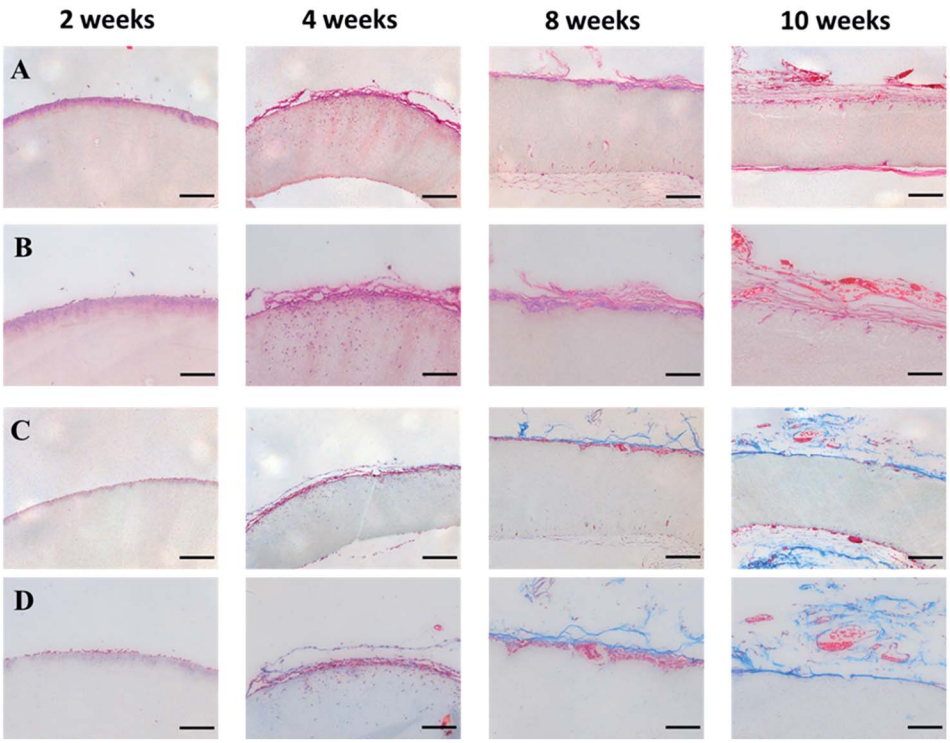

Fig. 7 Typical H&E staining (A and B) and Masson's trichrome staining (C and D) images of PLLA/PLCL (40 : 60) valve scaffolds after subcutaneous implantation for 10 weeks. (A and C) 100×, bar = 200 μm; (B and D) 200×, bar = 100 μm.

have no growth potential and do not exhibit regenerative potential. Therefore, an appropriate valve vascular is urgently needed to be developed and utilized.

In this study, a novel PLLA/PLCL nanofiber-based valve integrated scaffold was fabricated by a TIPS-based strategy combining with a 3D printing mold. The valve integrated tubular scaffold exhibited desirable mechanical properties and satisfied functional performance, supporting that the original strategy is an efficient process for manufacturing biomimetic valve scaffolds.

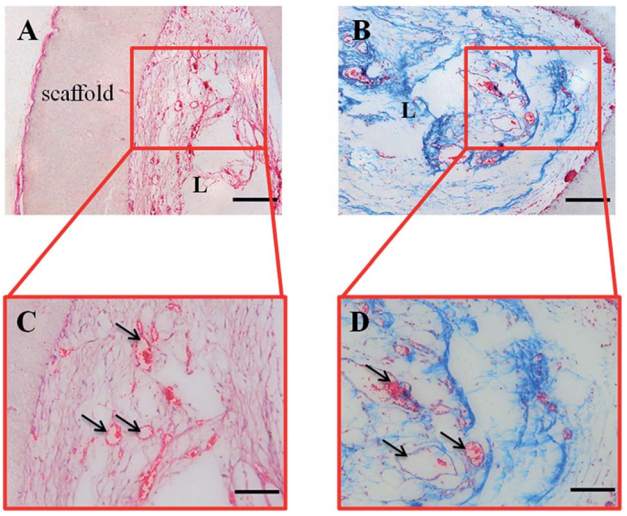

Fig. 8 H&E staining (A and C) and Masson's trichrome staining (B and D) images of representative new capillaries regeneration in PLLA/PLCL (40 : 60) valve scaffolds after subcutaneous implantation for 10 weeks. "L" indicates the lumen of valve scaffold. Arrows indicates new capillaries. (A and B) 100×, bar = 200 μm; (C and D) 200×, bar = 100 μm.

There are a lot of methods available for the fabrication of scaffolds with a controlled shape and pore architecture, such as three-dimensional (3D) printing, laser sintering, gas foaming, phase separation, electrospinning, *etc.*[12–14] Amongst these various engineering approaches, thermally induced phase separation (TIPS) is a facile way to prepare nanofibrous scaffolds.[28,29] The TIPS-based technique combined with controllably shape are increasingly gaining importance for satisfying special requirements for the microstructure and biofunction in tissue engineering and other related applications. Therefore, taking advantage of the characteristic of morphological plasticity, a valve integrated scaffold (Fig. 2A) was successfully obtained to mimic human pulmonary valved artery using TIPS based strategy.

Replicating morphology and geometry of the native tissue has been considered critical for manufacturing an appropriate valve vascular substitute. A specific mold could be used in a typical production process of TIPS, which could determine the original structure including shape and size of target valve conduit. For the most part, the mold obtained by traditional machining methods only processed simple shapes such as a cylindrical chamber mold.[30,31] However, it could not meet our requirements above. In our research, automated manufacturing technology (3D printing) was conducted to fabricate particular mold for a novel valve integrated scaffold with higher

anatomical precision, and this process can be rapidly accomplished by building a optimized computer aided design (CAD) models (Fig. 1A). Importantly, the property of completeness has been a major focus in engineering valve scaffolds for ensuring proper durability and hemodynamics. Therefore, a special mold with interspace between corolla-like compositions and covering conduit was designed to shape strong valve integrated scaffolds *via* TIPS-based technique. Moreover, by using special printing materials, all sections of the printed mold were transparent enough to acquire observed achievement at any time for more effective operation of experiment (Fig. 1B).

Polylactide and poly(L-lactide-*co*-caprolactone), as biocompatible and biodegradable polymers, have been applied frequently in biomedical engineering,[32,33] and approved by the FDA in clinic. PLLA/PLCL scaffolds exhibited a biomimetic nanofibrous structure and indicated their good compliance and resistance to permanent deformation as a potential vascular graft in the component ratio of 40 : 60, which was identified as the optimal candidate for tissue engineering application in terms of elastic properties and structural integrity.[15] In this study, PLLA/PLCL scaffold fabricated by TIPS-based technique showed excellent structural and mechanical properties, which was robust enough to prop up for artery blood flow in the use of pulmonary valved artery replacement. Hysteresis curves for multicycle loading–unloading fatigue cycles showed slight plastic deformations for PLLA/PLCL scaffold. Biomimetic structure is a key characterization for an ideal valve scaffold, because it could provide a biomimetic hemodynamics microenvironment to maintain the normal fluid of blood flow, especially in the unique position such as pulmonary artery.

Hemodynamics plays a vital role in driving and maintaining cardiovascular development.[34] *In vitro* experimental investigation is an essential to analyze valves dynamics and structure. CFD simulations have been employed to hemodynamic parameters estimation, *in vivo* blood characteristics and measurements, anatomically precise geometries and boundary layer conditions.[35] In our simulation, we used a physiological pulmonary artery flow velocity, which enables us to analysis flow phenomena in a bionic fluid environment, for imitating the particular subject like pulmonary artery. During corresponding diastolic phase, tri-leaflet valve was put into good use to block the regurgitation, which could efficiently lead relief of right heart ventricle when used by CHD patients. Besides, CSD-technique also exploited to assess the structure of every single leaflet. According to the results, the maximum deformation and stress were conceivably appeared at relative center of free edge. It was noteworthy that the corners of valve, where exactly were the conjunctions with valve and conduit wall, also overloaded with stress. This theory evidence could provide exactly guidance for design and further optimization of valve integrated scaffolds.

A biodegradable polymer-based scaffold must be able to maintain suitable degradation rates. PLLA/PLCL scaffold undergoes bulk degradation through hydrolysis of the ester linkages. After some time, the extent of crosslinking is decreased enough to allow for the outward diffusion of degradation products, resulting in a loss of mass and structural integrity of the scaffold. However, a long-term degradation experiment for the PLLA/PLCL scaffold would be worth implementing in further study.

In addition, our previous study has indicated the excellent biocompatibility of the scaffold, which demonstrated good cellular attachment, spreading, proliferation, and phenotypic maintenance for endothelial cells seeded PLLA/PLCL scaffolds.[15]

In vivo test is the most direct and effective way for biological evaluation of valve scaffolds. Cell infiltration is the initial step in subsequent regeneration and remodeling progress of vascular grafts in the long term, such as vascularization, ECM secretion and deposition.[36] Macroporous architecture is crucial for vascular scaffolds, which can provide sufficient space for cell migration, matrix deposition, and tissue formation.[37] Our results have confirmed this viewpoint from the *in vivo* aspect. After subcutaneous implantation of PLLA/PLCL scaffolds into nude mice, increased cellularity was observed in the explants, presumably reflecting the advantage of porosity and favorable biocompatibility of PLLA/PLCL scaffolds for future potential clinical applications. The success of regeneration requires matrix production by the cells *in vivo*. Our results also demonstrated an increased collagen concentrations and new capillaries regeneration, which showed the functionality of infiltrated cell and the neovascularization of PLLA/PLCL scaffolds *in vivo*. The developed valve integrated scaffold made a breakthrough for pulmonary valved artery prosthesis construction. Collagen production and tissue regeneration *in vivo* could overcome the restriction of a homograft valve conduit. Hence, such PLLA/PLCL scaffolds could be potential valve vascular substitutes for pulmonary valved artery replacement. Further transplantation research for the nanofibrous valve integrated grafts would be worth implementing in big animals.

Conclusions

In this study, we present a facile TIPS method to prepare a novel nanofibrous valve integrated scaffold with PLLA/PLCL in an optimal ratio of 40 : 60 as potential pulmonary valved artery substitute. The structure and architecture of the resultant valve integrated scaffolds could mimic native pulmonary valves, and the mechanical properties could afford the arterial pressure of pulmonary artery. The outcomes evaluated by the computational fluid dynamics (CFD) simulation system showed that regurgitation during corresponding diastolic phase was effectively blocked. Furthermore, the scaffolds exhibited abundant collagen production and new capillary regeneration after subcutaneous implantation for 10 weeks, suggesting the potential value of the novel PLLA/PLCL valve integrated scaffolds for complex congenital heart disease.

Acknowledgements

This work was supported by the National Natural Science Foundation of China [No. 81271726] [No. 81501558], Collaborative Innovation Center for Translational Medicine at

Shanghai Jiao Tong University School of Medicine [TM201504], The Project-sponsored by the Scientific Research Foundation for the Returned Overseas Chinese Scholars, State Education Ministry [No. 20144902], The Fund of The Shanghai Committee of Science and Technology [No. 14411968900]; The Project funded by China Postdoctoral Science Foundation [No. 2014T70420] and the Fund of Shanghai Jiao Tong University School of Medicine [No. 14XJ10039].

References

1 T. Breymann, W. R. Thies, D. Boethig, R. Goerg, U. Blanz and R. Koerfer, Bovine valved venous xenografts for RVOT reconstruction: results after 71 implantations, *Eur. J. Cardiothorac. Surg.*, 2002, **21**, 703–710.

2 Y. Bazilevs, J. C. del Alamo and J. D. Humphrey, From imaging toprediction: emerging non-invasive methods in pediatriccardiology, *Prog. Pediatr. Cardiol.*, 2010, **30**, 81–89.

3 B. J. Bellhouse, F. H. Bellhouse and K. G. Reid, Fluid mechanics of the aortic root with application to coronary flow, *Nature*, 1968, **219**, 1059–1061.

4 I. Vesely, Aortic root dilation prior to valve opening explained by passive hemodynamics, *J. Heart Valve Dis.*, 2000, **9**, 16–20.

5 P. Dagum, G. R. Green, F. J. Nistal, G. T. Daughters, T. A. Timek, L. E. Foppiano, A. F. Bolger, N. B. Ingels Jr and D. C. Miller, Deformational dynamics of the aortic root: modes and physiologic determinants, *Circulation*, 1999, **100**, II54–II62.

6 P. B. Matthews, A. N. Azadani, C. S. Jhun, L. Ge, T. S. Guy, J. M. Guccione and E. E. Tseng, Comparison of porcine pulmonary and aortic root material properties, *Ann. Thorac. Surg.*, 2010, **89**, 1981–1988.

7 J. T. Butcher, G. J. Mahler and L. A. Hockaday, Aortic valve disease and treatment: the need for naturally engineered solutions, *Adv. Drug Delivery Rev.*, 2011, **63**, 242–268.

8 A. N. Azadani, S. Chitsaz, P. B. Matthews, N. Jaussaud, J. Leung, A. Wisneski, L. Ge and E. E. Tseng, Biomechanical comparison of human pulmonary and aortic roots, *Eur. J. Cardiothorac. Surg.*, 2012, **41**, 1111–1116.

9 J. W. Brown, M. Ruzmetov, M. D. Rodefeld, P. Vijay and R. K. Darragh, Valved bovine jugular vein conduits for right ventricular outflow tract reconstruction in children: an attractive alternative to pulmonary homograft, *Ann. Thorac. Surg.*, 2006, **82**, 909–916.

10 J. Perron, A. M. Moran, K. Gauvreau, P. J. del Nido, J. E. Mayer Jr and R. A. Jonas, Valved homograft conduit repair of the right heart in early infancy, *Ann. Thorac. Surg.*, 1999, **68**, 542–548.

11 T. Wu, C. Huang, D. Li, A. Yin, W. Liu, J. Wang, J. Chen, H. Ei-Hamshary, S. S. Al-Deyab and X. Mo, A multi-layered vascular scaffold with symmetrical structure by bi-directional gradient electrospinning, *Colloids Surf., B*, 2015, **133**, 179–188.

12 H. N. Chia and B. M. Wu, High-resolution direct 3D printed PLGA scaffolds: print and shrink, *Biofabrication*, 2014, **7**, 015002.

13 N. Kasoju and U. Bora, Silk fibroin based biomimetic artificial extracellular matrix for hepatic tissue engineering applications, *Biomed. Mater.*, 2012, **7**, 045004.

14 R. Ahmadi, N. Mordan, A. Forbes and R. M. Day, Enhanced attachment, growth and migration of smooth muscle cells on microcarriers produced using thermally induced phase separation, *Acta Biomater.*, 2011, **7**, 1542–1549.

15 W. Wang, J. Hu, C. He, W. Nie, W. Feng, K. Qiu, X. Zhou, Y. Gao and G. Wang, Heparinized PLLA/PLCL nanofibrous scaffold for potential engineering of small-diameter blood vessel: tunable elasticity and anticoagulation property, *J. Biomed. Mater. Res., Part A*, 2015, **103**, 1784–1797.

16 J. P. Vacanti and R. Langer, Tissue engineering: the design and fabrication of living replacement devices for surgical reconstruction and transplantation, *Lancet*, 1999, **354**, SI32–SI34.

17 C. V. Bouten, P. Y. Dankers, A. Driessen-Mol, S. Pedron, A. M. Brizard and F. P. Baaijens, Substrates for cardiovascular tissue engineering, *Adv. Drug Delivery Rev.*, 2011, **63**, 221–241.

18 J. P. Vacanti, R. Langer, J. Upton and J. J. Marler, Transplantation of cells in matrices for tissue regeneration, *Adv. Drug Delivery Rev.*, 1998, **33**, 165–182.

19 L. Soletti, Y. Hong, J. Guan, J. J. Stankus, M. S. El-Kurdi, W. R. Wagner and D. A. Vorp, A bilayered elastomeric scaffold for tissue engineering of small diameter vascular grafts, *Acta Biomater.*, 2010, **6**, 110–122.

20 C. He, W. Feng, L. Cao and L. Fan, Crosslinking of poly(L-lactide) nanofibers with triallyl isocyanutrate by gamma-irradiation for tissue engineering application, *J. Biomed. Mater. Res., Part A*, 2011, **99**, 655–665.

21 C. He, G. Xiao, X. Jin, C. Sun and P. X. Ma, Electrodeposition on nanofibrous polymer scaffolds: rapid mineralization, tunable calcium phosphate composition and topography, *Adv. Funct. Mater.*, 2010, **20**, 3568–3576.

22 C. He, X. Xu, F. Zhang, L. Cao, W. Feng, H. Wang and X. Mo, Fabrication of fibrinogen/P(LLA–CL) hybrid nanofibrous scaffold for potential soft tissue engineering applications, *J. Biomed. Mater. Res., Part A*, 2011, **97**, 339–347.

23 W. He, Z. Ma, W. E. Teo, Y. X. Dong, P. A. Robless, T. C. Lim and S. Ramakrishna, Tubular nanofiber scaffolds for tissue engineered small-diameter vascular grafts, *J. Biomed. Mater. Res., Part A*, 2009, **90**, 205–216.

24 X. M. Mo, C. Y. Xu, M. Kotaki and S. Ramakrishna, Electrospun P(LLA–CL) nanofiber: a biomimetic extracellular matrix for smooth muscle cell and endothelial cell proliferation, *Biomaterials*, 2004, **25**, 1883–1890.

25 J. Wu, C. Huang, W. Liu, A. Yin, W. Chen, C. He, H. Wang, S. Liu, C. Fan, G. L. Bowlin and X. Mo, Cell infiltration and vascularization in porous nanoyarn scaffolds prepared by dynamic liquid electrospinning, *J. Biomed. Nanotechnol.*, 2014, **10**, 603–614.

26 J. E. Mayer Jr, Uses of homograft conduits for right ventricle to pulmonary artery connections in the neonatal period, *Semin. Thorac. Cardiovasc. Surg.*, 1995, **7**, 130–132.

27 R. A. Hopkins, *Resolution of the Conflicting Theories of Prolonged Cell Viability*, Springer, New York, 2005, pp. 184–189.

28 J. Hu, X. Sun, H. Ma, C. Xie, Y. E. Chen and P. X. Ma, Porous nanofibrous PLLA scaffolds for vascular tissue engineering, *Biomaterials*, 2010, **31**, 7971–7977.

29 C. Xie, J. Hu, H. Ma, J. Zhang, L. J. Chang, Y. E. Chen and P. X. Ma, Three dimensional growth of iPS cell-derived smooth muscle cells on nanofibrous scaffolds, *Biomaterials*, 2011, **32**, 4369–4375.

30 N. Kasoju, D. Kubies, T. Sedlačík, O. Janoušková, J. Koubková, M. M. Kumorek and F. Rypáček, Polymer scaffolds with no skin-effect for tissue engineering applications fabricated by thermally induced phase separation, *Biomed. Mater.*, 2016, **11**, 015002.

31 H. Ma, J. Hu and P. X. Ma, Polymer scaffolds for small-diameter vascular tissue engineering, *Adv. Funct. Mater.*, 2010, **20**, 2833–2841.

32 J. I. Lim and J. H. Kim, Enhanced biocompatibility and adhesive properties of modified allyl 2-cyanoacrylate-based elastic bio-glues, *Colloids Surf., B*, 2015, **133**, 19–23.

33 M. C. Tsai, K. C. Hung, S. C. Hung and S. H. Hsu, Evaluation of biodegradable elastic scaffolds made of anionic polyurethane for cartilage tissue engineering, *Colloids Surf., B*, 2015, **125**, 34–44.

34 B. P. Hierck, K. Van der Heiden, C. Poelma, J. Westerweel and R. E. Poelmann, Fluid shear stress and inner curvature remodeling of the embryonic heart. Choosing the right lane!, *Sci. World J.*, 2008, **8**, 212–222.

35 K. N. Bharadwaj, C. Spitz, A. Shekhar, H. C. Yalcin and J. T. Butcher, Computational Fluid Dynamics of Developing Avian Outflow Tract Heart Valves, *Ann. Biomed. Eng.*, 2012, **40**, 2212–2227.

36 P. Zilla, D. Bezuidenhuit and P. Human, Prosthetic vascular grafts: wrong models, wrong questions and no healing, *Biomaterials*, 2007, **28**, 5009–5027.

37 Z. Wang, Y. Cui, J. Wang, X. Yang, Y. Wu, K. Wang, X. Gao, D. Li, Y. Li, X. L. Zheng, Y. Zhu, D. Kong and Q. Zhao, The effect of thick fibers and large pores of electrospun poly(ε-caprolactone) vascular grafts on macrophage polarization and arterial regeneration, *Biomaterials*, 2014, **35**, 5700–5710.

